Population Variance in Pelvic Response to Lateral Impacts - A Global Sensitivity Analysis

Population Variance in Pelvic Response to Lateral Impacts – A Global Sensitivity Analysis

Erik Brynskog, Johan Iraeus, Bengt Pipkorn, Johan Davidsson

Abstract Pelvic fracture remains the third most common moderate to severe injury in motor vehicle crashes, and the dominating lower extremity injury in lateral impacts. An essential tool for analysis of injury, and real-world occupant protection, are finite element human body models. However, today's state-of-the-art pelvis models do not adequately consider the variability in shape and size naturally occurring in human populations. In this study, we developed a new detailed pelvis finite element model, morphable to enable representation of the population shape variance. The model was validated using force-displacement data from post-mortem human subjects, in lateral loading of the denuded pelvis, followed by a global sensitivity analysis.

The results suggests that in lateral impacts to the pelvis, pelvic shape contributes to the model response variance by the same magnitude as pelvic bone material stiffness, and that each of these contributions are approximately twice that of the cortical bone thickness. Hence, to model pelvic response for a general population accurately, future studies must consider both pelvic shape and the material properties in the analysis. Increased knowledge about population variability, and inclusion in safety evaluations, can result in more robust systems that reduce the risk of pelvic injuries in real-world accidents.

Keywords FE-HBM, lateral impact, pelvis, population variance, sensitivity analysis.

I. INTRODUCTION

Pelvic fracture is the third most common moderate to severe injury in motor vehicle crashes (MVCs) [1]. In lateral and oblique MVCs, pelvic fractures have been identified as the dominating moderate to severe lower extremity injury and an increased focus on predicting this type of injury has been called for [2]. Pelvic ring fractures specifically, are associated with the highest early mortality rate for patients with orthopaedic injuries, and some degree of residual disability can be expected regardless of treatment [3]. In addition, future automated vehicles might accentuate the risk of pelvis injury, given current injury data, since an increased ratio of intersection crashes, commonly involving lateral and oblique impacts, on the total number of MVCs is expected [4,5]. As a result, pelvic fracture prevention should be prioritised in both current and future vehicle safety systems.

A tool used to study injury via computer simulations are finite element (FE) human body models (HBMs). FE-HBMs can be used for detailed injury analysis and allow for a more realistic description of the human anatomy compared to mechanical models, like anthropometric test devices. Several pelvis FE-models for lateral impact evaluations exist in the literature [6–15]. However, most of these models target an average-sized male, while studies on the effect of population variability have been limited, especially in terms of variation in shape. If the analysis is limited to a single point (e.g., the average man), there is a risk that the restraint system will be sub-optimised and thereby less effective for the wider population. To address this potential issue, thorough validation and assessment of model sensitivity to input variations is essential [16–17]. Sensitivity analysis allows for consideration of not only the average, but also the distribution of possible outcomes due to variations for example in geometry, material, loading, and boundary conditions. In line with this, a current trend in the field of traffic safety FE-HBM development is to include in the analysis population variability, both on a material and geometrical level [18–21]. By broadening the analysis past the average sized male, optimisation of safety systems for a wider population is enabled.

Outside the field of traffic safety, notable efforts to study the sensitivity of pelvis FE-models include [22–23]. Reference [22] analysed a subject specific FE-model, subjected to body weight loading through the proximal femur. Varying their input parameters around this baseline, they concluded that cortical bone strains were most

Brynskog (erik.brynskog@chalmers.se; +46 (0)31-77 28 430) is a PhD student, J. Iraeus a Senior Researcher, B. Pipkorn an Adjunct Professor, and J. Davidsson an Associate Professor at the Division of Vehicle Safety, Chalmers University of Technology, Gothenburg, Sweden. B. Pipkorn is Director of Simulation and Active Structures at Autoliv, Vårgårda, Sweden.

sensitive to changes in cortical thickness and cortical bone elastic modulus, while deviation in other input parameters (like trabecular bone elastic modulus) had little effect on the predicted cortical strains. However, this study did not include variations in pelvis shape. Reference [23] studied a subject specific hemipelvis undergoing peak load during gait. They concluded that bone geometry was the most influential input parameter on acetabulum trabecular bone strain and that interaction between shape and trabecular bone elastic modulus was influential to the simulated strain response. However, the shape variations were only assessed by volumetric scaling. Neither of these studies considered high severity loading from lateral impacts.

The shape of the pelvic structure is complex. It consists of three separate bones, two innominate bones and sacrum, which form the pelvic ring. Sexually dimorphic measurements have been confirmed [24] and books on anatomy describe the female and male pelvis as strikingly different. Hence, a clear distinction between the average female/male pelvic shape should be expected, but since the range of most features overlap, the inter-individual differences can be more pronounced than the sex differences [25]. The population variance in pelvic shape is substantial, as verified by Sparse Principal Component Analysis (SPCA) [25], and could explain a significant portion of the response variance seen in post-mortem human subject (PMHS) testing [26–29].

In the assessment of model sensitivity, several sensitivity analysis methods exist in the literature, as summarised in [30–31]. These can broadly be distinguished as local, where one parameter at a time is varied, and global, where all parameters are varied simultaneously [32]. While being intuitive and easy to set up, local sensitivity analysis is only valid if the model is linear with no interactions and only explore a limited area of a multi-dimensional space. Global sensitivity analysis (GSA) on the other hand, is valid when the model response is both nonlinear and include interaction effects amongst parameters [32]. GSA is frequently performed using variance decomposition techniques, where the first-order and total sensitivity indices can be computed via Monte-Carlo (MC) simulations. However, while being considered a standard benchmark, the MC simulation method has a high computational cost making it unfeasible for complex models, like detailed FE models [33]. Alternative methods to approximate sensitivity indices at a much lower cost compared to MC have been suggested, including iterative designs [34], meta-modelling [35], and dimensional reduction methods (DRMs) [33], for example. These allow for an effective inclusion of population variance in computationally expensive FE-models.

The main aim of this study was to quantify the effect of population variance in both pelvic shape and material properties on the simulated response from the most critical pelvis loading in MVCs, i.e., lateral impacts. The sub aims were: (1) to validate a pelvis FE-model for lateral impact evaluations, and (2) to identify and rank the most influential shape variables on model response. The result of this study can be used to guide future research efforts and aid in the analysis of pelvic fracture prevention.

II. METHODS

A new detailed pelvis FE-model was built based on the average pelvic shape of 132 (75 females, 57 males) Computed Tomography (CT) scans from clinical imaging studies at the University of Michigan Department of Radiology, USA. A morphometric model previously published [25], predicting pelvic shape from overall anthropometry (sex, age, stature, Body Mass Index (BMI)) based on SPCA, was used to predict shapes of a 50th percentile female (50 years, 162 cm, and 63 kg) and male (50 years, 175 cm, and 77 kg). Morphing of the average FE-model to the predicted shapes was done with a radial basis function using thin-plate-splines interpolation [36]. The resulting models are displayed in Fig. 1 and are referred to as the baselines.

Model sensitivity to impactor force and strain in the superior pubic rami from lateral impacts to the acetabulum was studied by morphing the FE-model based on the SPCA results and including variations in cortical bone thickness and variations in cortical and trabecular bone material stiffness. Variations in boundary conditions were not considered. The FE-model was built in LS-DYNA (LST, Livermore, CA, USA) and all simulations were performed using MPP R11.1.0 Double Precision. For LS-DYNA specific information about element formulation, material models, and contact settings see Appendix A.

Fig. 1. Pelvis FE-models for the female baseline (left) and male baseline (right).

New Pelvis FE-model

Cortical thickness distributions of the innominate bone from 10 normal controls (5 females, 5 males) were analysed [37]. The subjects were morphed to the shape of the average pelvis, using the method presented in [25], and the thickness distribution was mapped to the FE-model using ANSA 21.1.1, Beta CAE Systems. The distribution of nodal thicknesses of each subject was found to be lognormal with a mean of 1.64 mm. Hence, a lognormal distribution was fitted to the nodal thicknesses of each subject, and the subject with a distribution closest to the average lognormal curve, was chosen as baseline, see Fig. 2. A uniform cortical thickness of 1.3 mm was assigned to the sacrum [38–39].

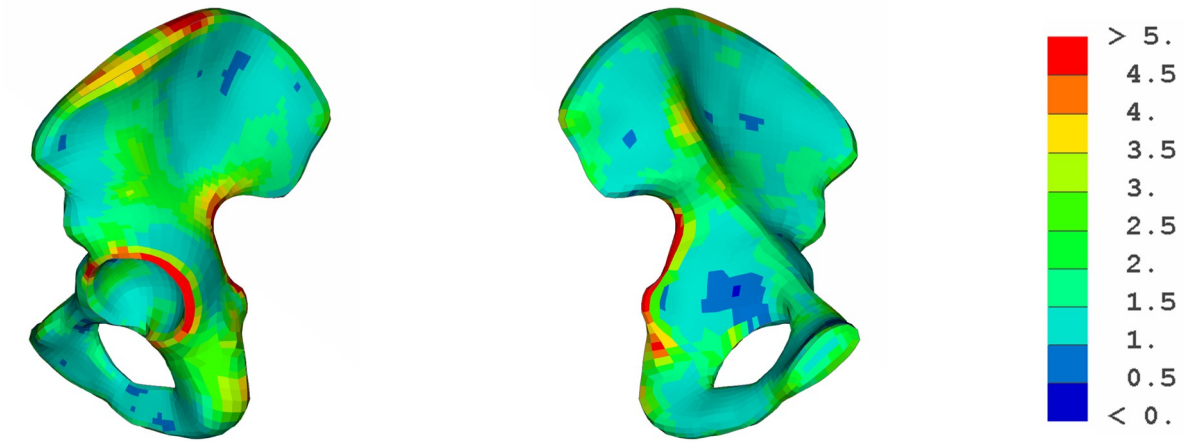

Fig. 2. Pelvis FE-model cortical bone thickness [mm] seen from lateral (left) and medial (right) views.

The average pelvis shape was defined on the outer cortical surface. To have a shell midplane in the middle of the cortical thickness, the nodes were offset inwards in the element normal direction by half the baseline thickness, locally evaluated for each node. Trabecular bone filled the new volume and was modelled using under integrated solid elements with an isotropic perfect-plastic material. In the baseline model, Young's-modulus was set to 70 MPa [40] and yield strain to 0.81% [41]. The cortical bone was modelled on the surface of the trabecular bone using fully integrated shell elements and a piecewise linear elastoplastic material. In the baseline model, Young's-modulus was set to 10.96 GPa, based on weighted average from [42], while average yield strain of 0.52% and plastic stress-strain response was computed by a linear elastic strain offset and cubic spline curve fitting on tracked stress-strain results [42], see Fig. 4. Element erosion to simulate bone fracture was not included in the model.

The pubic symphysis disc was modelled using fully integrated solids and a rubber material model, defined by a tension-compression stress-strain curve. The pubic symphysis ligaments were modelled on the surface of the disc using fully integrated shell elements and a material model similar to the disc. The thickness of the ligaments was uniformly set to 1 mm. The two stress-strain curves defining the materials were calibrated by simulating pubic symphysis component tests [43], see Appendix B for calibration results.

The sacroiliac (SI) joint was modelled using fully integrated solids for the interosseous ligaments and the

cartilage of the articulating surfaces while anterior, posterior, sacrotuberous, and sacrospinous ligaments were modelled as cable elements. Ligament material properties were taken from the literature [44], and were defined by stress-strain curves, while the properties defined for the articulating cartilage were the same as for the pubic symphysis disc, lacking alternative data. Dimensional data for the thickness of the articular cartilage and the cross-section area of the ligaments were taken from the literature [45–47]. The interosseous solids were tied to the innominate bone while a separate sliding contact (friction coefficient = 0.3) was defined for the articulating solids. The SI joint modelling approach was validated against SI joint component tests [48], see Appendix C.

The lunate surface of the acetabulum was modelled as a smooth sphere with a radius of 24.2 mm placed in the centre of the acetabulum rim [49]. Cartilage solid elements covering the lunate surface was extruded to a femur head with radius 22.7 mm [50]. The resulting half-moon shape of the cartilage had a surface area of 2,315 mm^2, similar to a reported average area of 2,294 mm^2 [51]. The material properties of the cartilage were approximated to be the same as for the pubic symphysis disc.

Experimental Data and Validation

Reference [27] performed quasi-static and dynamic lateral loading experiments on denuded pelvic bones. The aim of their study was to document the pelvis biomechanical behaviour and its injury thresholds in an isolated setting. Pelvic bones from 10 subjects (9 males, 1 female, age range 47 to 86 years) were first tested in non-injurious and injurious quasi-static scenarios, by applying load at a constant speed of 5 mm/min using a plate pressing on the iliac crest or a metallic ball fitted to the acetabulum. Subsequently, pelvic bones from 12 other subjects (6 males, 6 females, age range 62 to 81 years) were tested under dynamic loading using a drop tower. The impact was delivered to the acetabulum metallic ball by a falling mass (m = 3.68 kg, v = 4 m/s) via an 11 mm thick silicone padding.

To simulate the experimental scenario, the FE-model was oriented on its side and placed in a rigid box filled with solid hexahedral elements, with material properties of a low temperature alloy (Wood's metal [52]). The load was applied either via a rigid rectangular plate or a rigid sphere (m = 0.36 kg). The load cases are referred to as iliac quasi-static, acetabulum quasi-static, and acetabulum dynamic, see Fig. 3. In the quasi-static case, the load was applied at a constant speed of 2.5 mm/s, resulting in insignificant dynamic effects compared to the experiment load rate. For the dynamic case, the 11 mm thick silicone padding was modelled with hexahedral solids and a one-term Ogden function for B452 silicone at a strain rate of 40 s^{-1} [53]. The impact was delivered by a rigid plate (m = 3.68 kg, v = 4 m/s) on the top surface of the silicone padding, which transferred the force to the rigid sphere. Contact between the sphere and acetabulum was modelled with a sliding contact (friction coefficient = 0.1).

Validation was done by comparing experimental and simulated response distribution, using a two-sample Kolmogorov-Smirnov test ($\alpha < 0.05$), by comparing experimental and simulated mean, using a one-way ANOVA test ($\alpha < 0.05$), and by visual inspection. For each load case, 50 Latin-Hypercube samplings (LHS) around each baseline model using the parameter distributions presented in the next section were generated. In iliac quasi-static loading, the validation was done for reported stiffness at 500 N load, while for the acetabulum quasi-static loading, the validation was done for the reported load-displacement response at 500 N and when loaded until fracture. In acetabulum dynamic loading, the validation was done for the reported force-displacement response, impulse response, and stiffness (estimated by peak load over displacement at peak load).

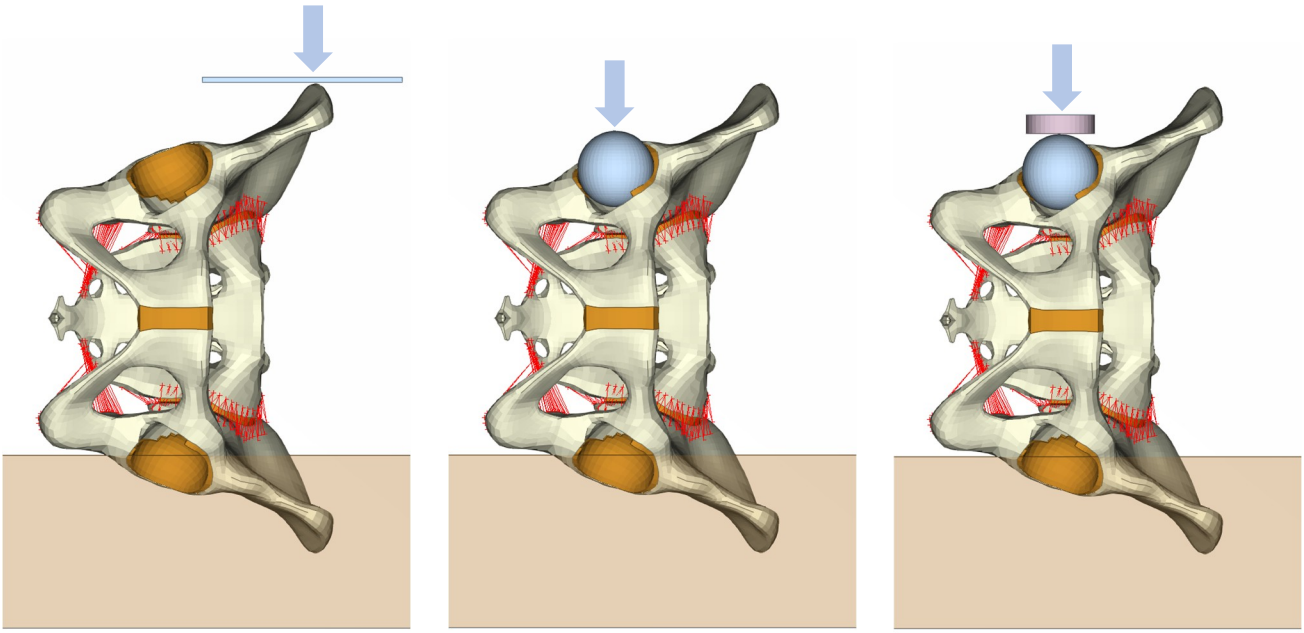

Fig. 3. Iliac quasi-static (left), acetabulum quasi-static (middle), and acetabulum dynamic (right).

Sensitivity Analysis

Response metric

The sensitivity analysis was performed for two separate response metrics, peak impactor force and strain in the struck side superior pubic rami. The peak impactor force was defined as the maximum resultant contact force between the rigid sphere and the acetabulum. The strain was defined for each node as the average effective plastic mid-plane strain of the connecting shell elements.

GSA method

Sensitivity analysis aims to quantify the contribution of each input variable on the random response of a system. A common approach is based on variance decomposition, where the total variance of the response is defined by the sum of the contribution of each input variable. Given a function $Y = h(\boldsymbol{X})$, where $\boldsymbol{X} = [X_1, X_2, \dots, X_n]^T$ are n independent random variables, the total variance V_Y of the response can be decomposed as

$$V_Y = \sum_{i=1}^{n} V_i + \sum_{i<j} V_{ij} + \cdots \tag{1}$$

where V_i is the variance from variable X_i, V_{ij} is the variance due to the interaction of variables X_i and X_j, and the dots represent higher order (more than two variables) interactions, as presented by [33]. Dividing Eq. 1 with the total variance V_Y, one obtains the Sobol's sensitivity indices as

$$1 = \sum_{i=1}^{n} S_i + \sum_{i<j} S_{ij} + \cdots \tag{2}$$

where S_i is referred to as the primary (or first-order) sensitivity index. For a model with no interaction between input variables, $\sum S_i$ equals one since all higher-order terms are zero, for all other cases $\sum S_i < 1$.

The most effective method for global sensitivity analysis of a general response function is MC simulations [33]. However, the method is time consuming and typically require tens of thousands of model evaluations, making it unrealistic for computationally demanding models. An approximation for variance-based GSA with sensitivity indices called the multiplicative dimensional reduction method (M-DRM), first proposed by [33], was used in this study. The method approximates high-dimensional integrals associated with the variance analysis by a product of one-dimensional functions. The original function $Y = h(\boldsymbol{X})$ is approximated as

$$h(\boldsymbol{X}) \approx h_0^{1-n} \cdot \prod_{i=1}^{n} h(X_i, \boldsymbol{C}_{-i}) \tag{3}$$

where the i^{th} univariate function is defined by fixing all input variables, but X_i, to the cut point $\boldsymbol{X} = \boldsymbol{C}$. Detailed information about the theory and implementation of M-DRM are omitted and referred to the original source but using Eq. 3, the primary sensitivity indices can be approximated as

$$S_i \approx \frac{\theta_i/\rho_i^2 - 1}{(\prod_{k=1}^{n} \theta_k/\rho_k^2) - 1} \tag{4}$$

where ρ_i and θ_i are one-dimensional integrals. As such, these can be computed numerically by Gaussian quadrature as

$$\begin{aligned} \rho_i &= \int_{X_i} h(X_i, \boldsymbol{C}_{-i}) f_i(X_i) dX_i \approx \sum_{j=1}^{N_{GP}} w_{ij} h(X_i^j, \boldsymbol{C}_{-i}) \\ \theta_i &= \int_{X_i} [h(X_i, \boldsymbol{C}_{-i})]^2 f_i(X_i) dX_i \approx \sum_{j=1}^{N_{GP}} w_{ij} \left[h\left(X_i^j, \boldsymbol{C}_{-i}\right)\right]^2 \end{aligned} \tag{5}$$

where $f_i(X_i)$ is the distribution function for parameter X_i, $\boldsymbol{C}_{-i}$ is the cut point vector with all variables but X_i fixed to their nominal values, $h(X_i^j, \boldsymbol{C}_{-i})$ is the functional evaluation for each input variable, and w_{ij} are Gaussian quadrature weights. Using Gaussian quadrature with N_{GP} Gauss-points and n variables the total number of simulations are at most nN_{GP}, which is several orders of magnitude less than the MC method.

Variables and distributions

The morphometric model implemented with the pelvis FE-model was generated based on 15 principal components (PCs) and one scale parameter [25]. These captured 89.8% of the total shape variance of the 132 subjects included (75 females, 57 males). A one-sample Kolmogorov-Smirnov test ($\alpha < 0.05$) could not reject that all shape related variables come from a normal distribution. Distributions in shape were defined based on the residual error around the predicted female/male baselines. The morphometric model with overall anthropometry (sex, age, stature, BMI) as independent variables only include PCs that were significantly captured. The residual was hence defined by standard error (SE) of the regression line for shape variables included in the morphometric model and by standard deviation (SD) of the entire sample for shape variables that were excluded, see TABLE I.

The Young's-modulus of trabecular bone was determined by an elasticity-density relationship [54]. A homogeneous Young's-modulus of 70 MPa, suggested by [40], was used as baseline resulting in an apparent density of 0.26 g/cm^3. Since no reference describing the distribution of apparent density in the trabecular bone of the pelvis was found, 87 samples of L3/L4 human vertebrae obtained from 23 subjects [55] were analysed. The range of the L3/L4 sample [0.10-0.43] g/cm^3 and mean 0.22 g/cm^3 was similar to the average and range in the pelvis study defining the elasticity-density relationship [54] (range 0.11-0.50 g/cm^3 and mean 0.24 g/cm^3, when excluding subchondral bone samples). The L3/L4 sample of apparent density was found to be lognormally distributed with SD = 0.064 g/cm^3, which was used to define the distribution around the baseline, see TABLE I.

Available data on Young's-modulus for the pelvic cortical bone is limited [42]. However, coupon testing of rib cortical bones have revealed normal distribution in Young's-modulus [56–58], which was assumed true also for the pelvic cortical bone. The SD of the distribution (1.85 GPa) was computed as the pooled SD from the pelvic coupon groups reported by [42]. The weighted average of the coupon groups (10.96 GPa) was used as baseline while the plastic stress-strain curve was scaled by the ratio between yield stress and baseline yield stress assuming a constant yield strain of 0.52%, see Fig. 4 and TABLE I.

The population distribution of cortical thickness in the innominate bone was estimated based on ten samples provided by [37]. A lognormal fit was made to each subject and a one-sample Kolmogorov-Smirnov test ($\alpha < 0.05$) could not reject that the lognormal parameter μ comes from a normal distribution with SD = 0.134. Thus, scaling of the cortical thickness of each node was performed as per Eq. 6:

$$T_{scaled} = e^{\ln(T) + Z\mu_{SD}} \tag{6}$$

where T_{scaled} is the computed thickness at each node, T is the baseline thickness of that node, Z is a standard normal distribution, and μ_{SD} is the SD of the lognormal parameter μ, see Fig. 5 and TABLE I. This is repeated for all nodes representing the cortical bone.

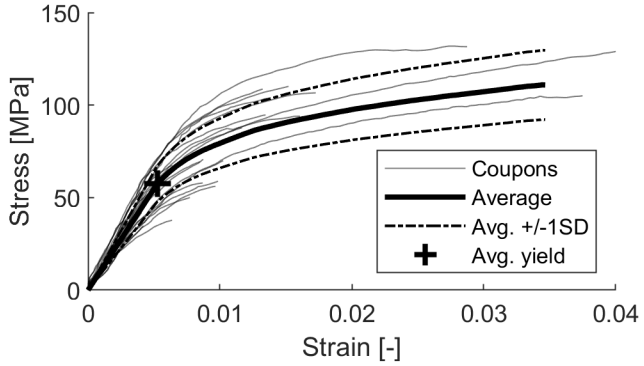

Fig. 4. Cortical bone material curves from coupon data [42], with baseline chosen as the average curve and distribution indicated by ±1SD.

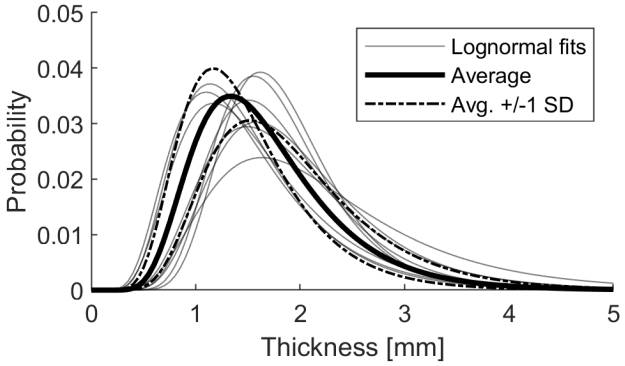

Fig. 5. Lognormal fits of cortical thickness to each subject, with baseline chosen as the most average and distribution indicated by ±1SD.

TABLE I

VARIABLE DISTRIBUTIONS. REGRESSION PREDICTED VARIABLES ARE SHOWN WITH TWO MEAN VALUES (FEMALE/MALE BASELINE) AND STANDARD ERROR OF THE REGRESSION INSTEAD OF STANDARD DEVIATION. SEE [25] FOR FURTHER DETAILS ABOUT SHAPE VARIABLES AND VISUAL REPRESENTATIONS.

Variable	Description (including main shape effect)	Distribution	Mean-value	SD or SE (*)
1	PC1 – Curvature of sacrum	Normal	-115.6 / 278.6	306.9*
2	PC2 – Length of sacrum	Normal	0	257.5
3	PC3 – Height of pelvis and transverse width of inlet	Normal	99.9 / -179.6	251.4*
4	PC4 – Width of ischial tuberosities	Normal	-302.0 / 360.4	243.8*
5	PC5 – Rotation of sacral endplate	Normal	-76.7 / 131.0	277.3*
6	PC6 – Inf-sup position of sacral endplate	Normal	0	392.3
7	PC7 – Ant-post diameter of inlet, thickness of pubic bones	Normal	39.5 / -16.9	178.4*
8	PC8 – Angle between pubic bone and ASIS	Normal	0	163.7
9	PC9 – Twist around vertical axis	Normal	0	139.3
10	PC10 – Curvature and length of lower sacrum (coccyx)	Normal	-89.3 / 219.3	244.9*
11	PC11 – Posterior bispinous breadth	Normal	-91.4 / 82.2	143.3*
12	PC12 – Size of iliac wing	Normal	0	248.6
13	PC13 – Width at acetabulum	Normal	0	136.6
14	PC14 – Lateral tilt of iliac wings, transverse width of inlet	Normal	0	248.4
15	PC15 – Inf-sup position of ischial tuberosities	Normal	-108.3 / 142.3	137.1*
16	Scale – Volumetric scaling (size)	Normal	1.020 / 0.998	0.0385*
17	Trabecular bone apparent density	Lognormal	0.26 g/cm^3	0.064 g/cm^3
18	Cortical bone Young's-modulus	Normal	10.96 GPa	1.85 GPa
19	Cortical bone thickness, lognormal μ parameter	Normal	[-]	0.134

III. RESULTS

Model Properties

The mesh of the model was made entirely of hexahedral solids (n = 23,926), quadrilateral shells (n = 10,984), and 1-D cable (n = 318) elements, with a target element side length of 3 mm. A high-quality mesh was prioritised to allow morphing of the model without risking severely distorted elements. See Appendix D TABLE D I and TABLE D II for mesh quality criteria used when developing the average model and resulting mesh quality of the average and female/male baseline models. For the average model all elements fulfilled the strict 100% limit. The morphed female/male baselines showed a minor decrease in mesh quality compared to the average geometry.

Calibration and Validation

Calibration and validation of pubic symphysis and SI joint properties using data from component experiments are presented in Appendix B and Appendix C.

Validation of the model response to lateral loading was done by a total of 306 simulations (51 simulations, one baseline and 50 LHS, for each sex and for each of the three load cases; iliac quasi-static, acetabulum quasi-static, and acetabulum dynamic). In the iliac quasi-static case, see Fig. 6 a), a one-way ANOVA ($\alpha < 0.05$) test showed that the difference between experiment and simulation mean response at 500 N were statistically different. In the acetabulum quasi-static case, see Fig. 6 b), the NULL hypothesis that the experiment and simulated stiffness at 500 N come from the same distribution could not be rejected (two-sample Kolmogorov-Smirnov test, $\alpha < 0.05$) and no statistically significant difference between the experiment and simulation mean was found (one-way ANOVA, $\alpha < 0.05$). When loading until fracture, see Fig. 7, the stiffness corridor was wider for the simulations than for the experiments but covered the complete range. The female baseline was close to average that of the experiments, while the male baseline followed the stiffest subject.

In the acetabulum dynamic case, the results were similar to the groups defined in the original experiments as non-fracturing or only anterior fractures, see Fig. 8 a) and b). For stiffness evaluated as max. load over displacement at max. load, see Fig. 8 c), the NULL hypothesis that the experiment and simulated response came from the same distribution could not be rejected (two-sample Kolmogorov-Smirnov test, $\alpha < 0.05$) and there was no statistically significant difference between the experiment and simulation mean (one-way ANOVA, $\alpha < 0.05$). The response post fracture deviates between simulation and experiments since the model does not simulate fracture using element erosion, see Fig. 8 d) after approximately 6ms and lack of complete fracture in Fig. 8 b).

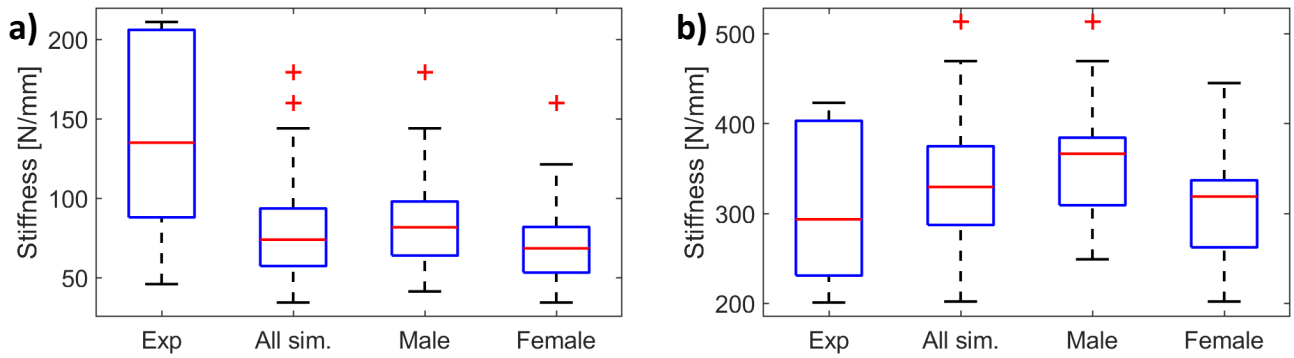

Fig. 6. Quasi-static stiffness at 500 N with load applied to the iliac wing (a) and to the acetabulum (b). Red solid line indicate mean, bottom and top edge of blue box indicate 25th and 75th percentiles respectively, black whiskers extend to most extreme value not considered outlier, and red plus signs indicate outliers.

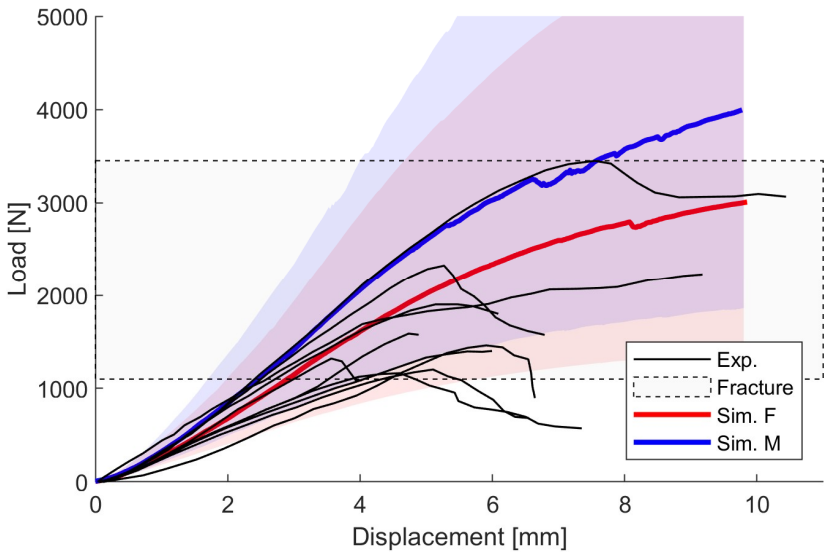

Fig. 7. Quasi-static load applied to the acetabulum as a function of resulting loading device displacement (experiment loaded until fracture).

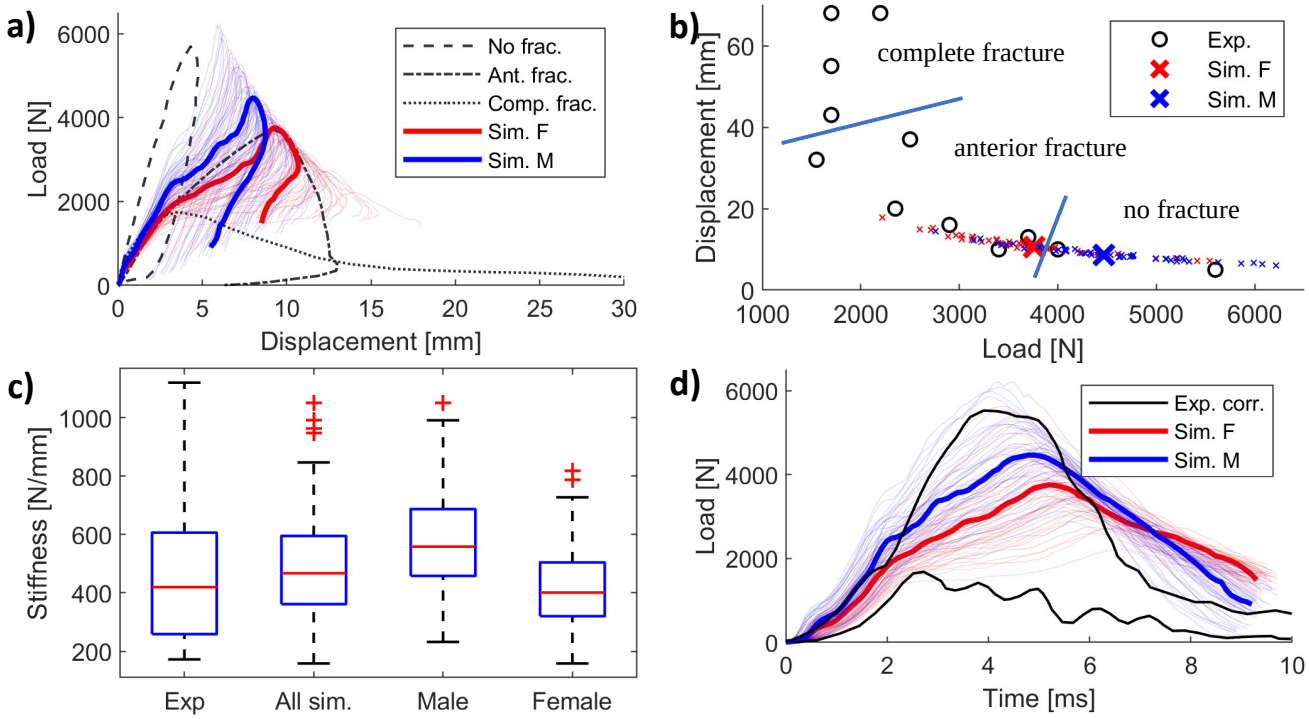

Fig. 8. Dynamic acetabulum response: a) force - displacement vs. three examples from experiments corresponding to non-fracturing, anterior fracture, and complete fracture, b) max. displacement - max. force vs. experiments, c) stiffness computed as max. force over displacement at max. force, d) impulse response vs. corridor from experiments.

Sensitivity Analysis

A total of 156 simulations of the dynamic load case were completed for the M-DRM sensitivity analysis. This corresponds to 5-point Gaussian integration with a Gauss-Hermite quadrature rule evaluated at [-2.86, -1.36, 0, +1.36, +2.85] SD for each variable. A 3-point quadrature was also performed to check convergence of the numerical integration. This resulted in similar ranking of all variables and a maximum difference of 1% for the summarised shape/material primary sensitivity indices. The average peak impactor force was 3.8 / 4.5 kN for the female/male models respectively (range: [2.4 – 4.9] / [2.9 – 5.8] kN). The average peak effective plastic strain was 5.3 / 3.3% (female/male, range: [2.1 – 11.3] / [0.9 – 7.9]%). The summation of primary sensitivity indices was 0.99 / 0.99 (female/male) for impactor force response and 0.93 / 0.88 (female/male) for effective plastic strain response, indicating that almost no interaction effects between variables exist when studying impactor force, while roughly 10% of strain response variance could be attributed to interaction effects, see Fig. 9 and Fig. 10.

Fig. 9 shows that the most important factors alone were cortical bone Young's modulus (Variable 18) and cortical bone thickness (Variable 19), for both impactor force and strain response. The most influential shape variables were Variable 3 (height of pelvis and transverse width of inlet), Variable 7 (anterior-posterior diameter of inlet and thickness of pubic bones), and Variable 14 (lateral tilt of iliac wings and transverse width of inlet).

Fig. 10 shows that when summarising the response variance contribution from shape (Variable 1-16) and material stiffness (Variable 17-18) separately, the shape effect was 34-38% while the material stiffness effect was 37-41%, depending on if the response metric evaluated was impactor force or cortical strain and if the baseline model was female or male. The variable controlling cortical bone thickness (Variable 19) contributed by 13-24%. This shows that pelvic shape contributes to the model response variance by the same magnitude as pelvic bone material stiffness, and that each of these contributions are approximately twice that of the cortical bone thickness. Fig. 10 also shows that for a strain-based response metric, a higher degree of interaction between input variables (≈10%) could be expected compared to a force-based response metric (≈1%).

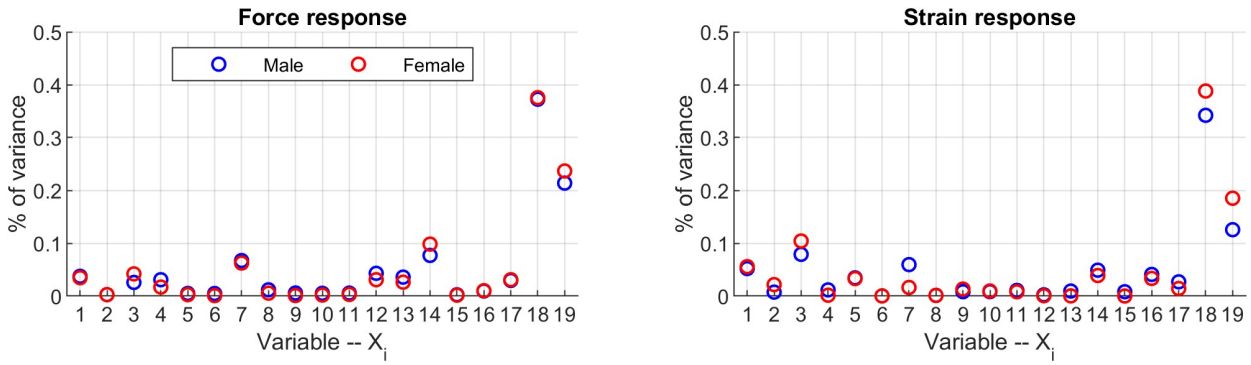

Fig. 9. Primary sensitivity indices for the female/male baseline model using peak impactor force (left) and nodal averaged effective plastic strain in the superior pubic rami (right) as evaluation metric. Variable 1-15 = PC1-15, Variable 16 = scale, Variable 17 = trabecular bone apparent density (used to compute Young's modulus), Variable 18 = cortical bone Young's modulus, and Variable 19 = cortical thickness.

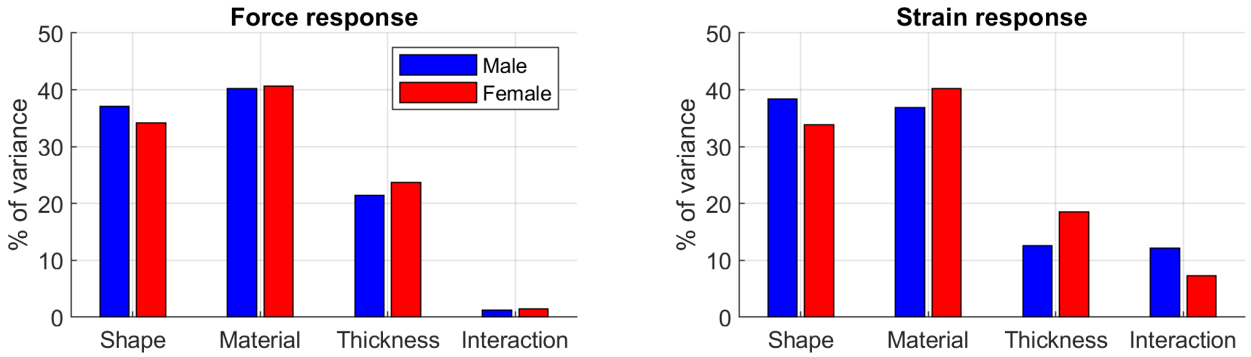

Fig. 10. Summation of primary sensitivity indices relating to shape (Variable 1-16), material stiffness (Variable 17-18), and cortical thickness (Variable 19), together with remaining interaction effects for a female/male baseline model using peak impactor force (left) and nodal averaged effective plastic strain in the superior pubic rami (right) as evaluation metric.

IV. Discussion

In this study, a detailed pelvis FE-model, capable of including population variance from both material properties and pelvic shape, was developed, calibrated, and validated. A high quality hexa/quad base mesh resulted in a robust and numerically stable model for a great variety of pelvic shapes achieved by morphing. The model was validated in terms of stiffness to previously published PMHS tests [27] and it was shown that when sampling from the proposed parameter distributions around an average female / male baseline, the model was able to capture the response reported in the experiments from lateral loading to the acetabulum. With the validated model, a global sensitivity analysis revealed that pelvic shape contributes to the model response variance by the same magnitude as the bone material stiffness. To the authors' knowledge, this is the first study to quantify the relative importance of shape and material input variables to the simulated response from lateral impacts to the pelvis.

Similar to previous studies [22], cortical strain was found to be sensitive to variations in cortical bone material stiffness, explaining 39 / 34% of response variance for the female/male model, and in cortical bone thickness, explaining 19 / 13% (female/male) of response variance. As in [22], the cortical strain was not particularly sensitive to variations in trabecular bone stiffness which explain 1 / 3% (female/male) in response variance. In addition, similar results were found for peak impactor force. Furthermore, the results of the current study indicate that response variance due to shape (≈35-40%) is of similar magnitude to variance due to cortical bone material stiffness, as shown in Fig. 10. This motivates future studies on pelvic bone material properties, given the lack in the current literature [42], while also highlighting the importance of publishing more details about the subject shape rather than just overall anthropometry in future PMHS testing.

Experimental studies of lateral impacts to the hip using PMHSs have shown significant spread in fracture tolerance [26–29]. As an example, [26] performed 60 impacts to 22 PMHs in a seated position using a rigid

spherical impactor centred on the greater trochanter. They found a force tolerance of 10 kN for the 50th percentile male subject and close to 4 kN for the 5th percentile female and concluded that the value of the tolerable impact force varies greatly with anthropometry. While overall anthropometry (sex, age, stature, BMI) has shown to be a poor predictor of pelvic shape, capturing only 29% of the total variance, substantial interindividual differences have been demonstrated [25]. The current study confirms the conclusions by [26] and quantifies the effect by presenting how much of the predicted response variance is attributed to the pelvic shape (≈35-40%), when sampling from a random distribution around an average baseline. To visualise the effect of the random distribution in shape, the weakest and stiffest model from the LHS used for validation can be seen in **Error! Reference source not found.**.

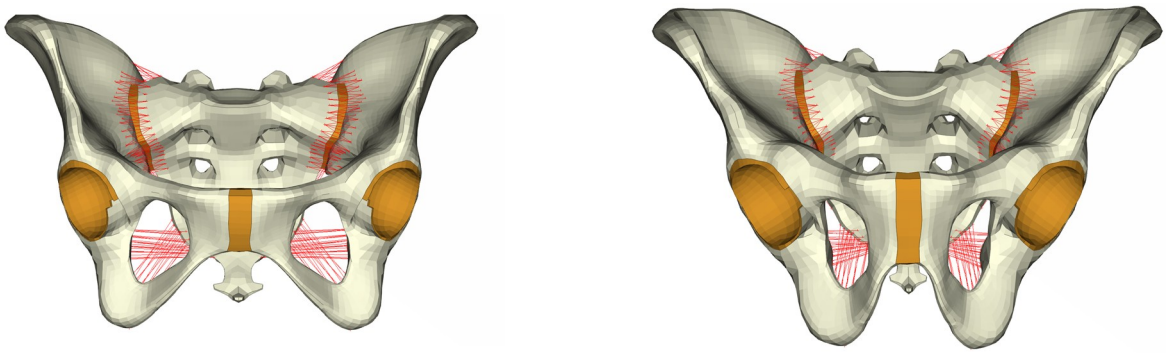

Fig. 11. Weakest (left) and stiffest (right) model from LHS used for validation. The resulting stiffness was achieved by a random sampling of both shape and material properties.

Two evaluation metrics were defined for the sensitivity analysis, peak impactor force and nodal averaged effective plastic strain. The force metric was chosen for two reasons. First, to enable extrapolation of the results to PMHS studies on pelvic response to lateral loading, where applied force is typically reported. Second, since the force response was considered more reliable given that the validation was conducted for force-displacement, rather than for strain. The strain metric was chosen to give guidance to future PMHS and/or simulation studies, seeking to study risk of fracture from lateral loading to the pelvis, even though the model was not validated for strain response. Analysing strain is motivated since a local criterion for fracture in human cortical bone is consistent with a strain-based criterion, as demonstrated experimentally [59–60]. This has been utilised in prior studies using 1st principal strains [61–62] and effective plastic strain [63–64]. In lateral compression of the pelvis, the superior pubic rami have been shown to be the primary location of initial fracture, followed by potential fractures to the posterior pelvis [26],[65–66]. Since the loading of the superior pubic rami was mainly from compression and bending, effective plastic strain was chosen over 1st principal strain. This metric has been shown to capture compression fracture location at onset of a compressive fracture using a cervical spine model [64]. To check the sensitivity of this assumption, the same analysis was performed using 1st principal strain and effective (total) strain with similar conclusions for the relative importance of different parameters, see Appendix E. Furthermore, to avoid a response that was highly sensitive to the quality of a single element, the strain was defined for each node as the average strain of the connecting elements. Hence, the metric extracted from each simulation for the strain-based sensitivity analysis was maximum nodal averaged effective plastic strain in the midplane of the cortical bone for the struck side superior pubic rami.

Both the validation and the sensitivity analysis were performed using the residual variance around a predicted average female/male baseline. This means that shape effects highly correlated to sex, age, stature, and BMI, will have a lower variance in the analysis than if the sampling would have considered the entire population without restrictions. For example, 65% of the population variance in Variable 4 (which controls the width of the ischial tuberosities and hence the sub-pubic angle) was captured by the morphometric model and was mainly correlated with sex. Would the study instead have been based around a single average pelvis, and the total variance included, the effect of this component would likely increase. This would be the case for all predicted shape components meaning that the response variance due to shape variations would be greater if considering only the average pelvis without differentiation based on sex. However, since the shape of female and male pelvises are markedly different, one could argue that they should be considered as separate cases and that combining the two would artificially increase the variance due to shape. Similarly, scale was significantly captured by stature

which means that the sampling performed neglects some of the total population variance in scale which can be attributed to variance in stature. Hence, would the study have included variance in age, stature, and BMI, instead of just the average anthropometry of the female/male baseline, the effect of shape would likely be even more pronounced.

The model passed the validation for acetabulum loading, which was the main focus of the sensitivity analysis. However, it did not pass the validation from iliac wing quasi-static loading, which is a limitation with the model. The reason for this is believed to be a lack of rotational stiffness in the pubic symphysis joint. In acetabulum loading the deformation of the pubic symphysis is mainly compression, which was well captured in the calibration, but for pure iliac loading the main deformation was a rotation of the joint in the medial plane. Future work should aim to improve the rotational stiffness of this joint. Furthermore, the model was not validated against strain data since [27] did not present strain in their paper. The absolute strain value from the simulations could hence be considered somewhat unreliable. However, this study does not compare the computed strain against an absolute value but rather looks at how this measure varies if the input variables change. As such, the conclusions regarding the contribution of different variables to the model response would remain as long as the strain distribution is consistent, regardless of a difference in absolute values. In addition, the validity of effective plastic strain as predictor for fracture in the superior pubic rami from lateral load has not been evaluated. Since effective plastic strain has been utilized in other studies [63–64] it was also chosen for the current evaluation, however further research is warranted.

One of the main challenges with sensitivity analyses is the variable distribution and potential correlations. Knowledge about how a variable varies within a population, and which distribution it follows, is often lacking and some assumptions are required. In this study, the shape variables are described using normal distributions which were found from a sample of 132 subjects [25]. The reliability of this distribution requires that these subjects can be considered a viable representation of the general population. The sample was drawn from a US population and was shown to compare with a modern US population in terms of overall anthropometry [25], but further generalisation based on ethnicity, for instance, is not possible. Regarding correlation, the shape variables presented were found by SPCA, which by design generates components that are orthogonal in space. This means that there is no correlation amongst the shape variables used. However, it is not known whether correlation exists between shape, cortical thickness, and material properties. To date, available data are insufficient to make such claims and no correlation was hence assumed for the current study.

The cortical thickness baseline was chosen as the subject with a thickness distribution closest to the average distribution, from a pool of ten normal controls [37], while the population distribution was defined by studying the lognormal fits of the same ten subjects. Only using ten subjects to define the distribution of the population is a limitation of the study. Furthermore, this method does not account for regional variations in cortical bone thickness between subjects and only works as a form of scaling for the chosen baseline.

The cortical bone material properties were defined using the only known coupon test made on pelvic cortical bone [42]. The [42] study is limited in that it only includes four subjects for a total of 20 coupons, they were all male, and coupons were extracted from different locations and orientations without tracking the osteon orientation. Two studies [57–58], on tensile and compressive loading of rib cortical coupons, have shown no significant difference in cortical stiffness between sexes, but it is unknown if this holds true for the pelvic bone as well. Age on the other hand, was found to be negatively correlated with material properties in tension [57], while no correlation was found in compression [58]. In addition, osteon orientation is known to affect the material properties of bone [67] but, to the authors' knowledge, no study currently exists showing a map of the osteon orientation over the pelvic cortical bone surface. Anisotropic and asymmetric material properties have been shown to improve fracture predictability in bone [68] and would be a great addition to future models, but further experimental studies are needed. The cortical bone Young's modulus implemented for the current study (mean = 10.96 GPa, SD = 1.85 GPa) is lower than what has been reported for rib coupons (mean ≈ 14.5 GPa and SD ≈ 3.5 GPa in tension [57], mean ≈ 12 GPa and SD ≈ 1.7 GPa in compression [58]) and femur coupons (mean ≈ 17 GPa and SD ≈ 3.0 GPa in tension/compression [69]. A possible explanation for this discrepancy is that the rib and femur values correspond to testing along the osteons, making them stronger, while the pelvic coupons were extracted with varying orientation. Regarding the distribution, reference [69] states that the Young's modulus is associated with a standard deviation of approximately 15-20%, consistent with what was implemented for the current study. In conclusion, whether or not the cortical bone material properties can be considered a true representation of

the population can be questioned and should be seen as a study limitation.

The trabecular material properties were defined as isotropic and homogeneous using the elasticity-density relationship presented by [54]. This is a simplification since apparent density is known to vary significantly within the pelvic trabecular bone, especially towards the roof of the acetabulum. In addition, since [54] did not provide estimates for the distribution of apparent density, a study on lumbar vertebrae trabecular bone [55] was used as proxy for this analysis. Furthermore, the methods used by [54] have later been shown to underpredict trabecular bone stiffness [70]. However, since the elasticity-density relationship seem to be dependent on the body region for which it was generated [71], and this is the only available relationship for the pelvic trabecular bone, it was still implemented. Given that the cortical bone is approximately two orders of magnitude stiffer than the average trabecular bone, and that previous studies have shown a limited influence on cortical strain due to variations in trabecular bone elastic properties [22], these simplifications were considered justified. In total, the validity of the trabecular bone material properties should be considered a limitation for the current study, and future research on pelvic trabecular bone material data is warranted.

The M-DRM computed sensitivity indices are approximations, relying on that a complex function of random variables can be approximated by a product of one-dimensional functions. The method also assumes that the sensitivity of the model can be estimated based on a fixed reference (or cut) point. Reference [33] demonstrates that these assumptions make for a good approximation of sensitivity indices, at a much lower computational cost, for a number of numerical examples using standard benchmark functions. A requirement for this to hold is that sufficient number of Gauss-points are used when performing the numerical integration. In this study, 3 and 5-point integration was evaluated to confirm that the solution had converged; the results presented were based on the 5-point integration.

V. CONCLUSIONS

A detailed pelvis FE-model, capable of including population variance from both material properties and pelvic shape, was developed, calibrated, and validated for lateral loading to the acetabulum. The results of this study suggest that pelvic shape contributes to the model response variance by the same magnitude as pelvic bone material stiffness, and that each of these contributions are approximately twice that of the cortical bone thickness, in simulated lateral impacts. Hence, to model pelvic response for a general population accurately, it is important for future studies to consider both the material properties and the pelvic shape in the analysis. Increased knowledge about population variability, and inclusion in safety evaluations, can result in more robust systems that reduce the risk of pelvic injuries in real-world accidents.

VI. ACKNOWLEDGEMENT

This work was carried out at SAFER – Vehicle and Traffic Safety Centre at Chalmers, Gothenburg, Sweden. The study was financed by FFI (Strategic Vehicle Research and Innovation, Award Number: 2018-04998), by VINNOVA, the Swedish Transport Administration, the Swedish Energy Agency, and the Swedish vehicle industry. The project partners are Chalmers University of Technology, Autoliv, Volvo Cars, and Sahlgrenska University Hospital. The simulations were performed on resources at Chalmers Centre for Computational Science and Engineering (C3SE) provided by the Swedish National Infrastructure for Computing (SNIC). All organisations are based in Sweden.

VII. REFERENCES

1. Weaver AA, Barnard RT, Kilgo PD, Martin RS, Stitzel JD. Mortality-based Quantification of Injury Severity for Frequently Occurring Motor Vehicle Crash Injuries. In: *Proceedings of the AAAM Annual Conference*. Québec City, Canada; 2013:235–46.
2. Pipkorn B, Iraeus J, Lindkvist M, Puthan P, Bunketorp O. Occupant injuries in light passenger vehicles—A NASS study to enable priorities for development of injury prediction capabilities of human body models. *Accident Analysis and Prevention* 2020; **138**. doi:10.1016/j.aap.2020.105443.
3. Tile M, Helfet DL, Kellam JF, Vrahas M. *Fractures of the Pelvis and Acetabulum - Principles and Methods of Management*. 4th ed. Georg Thieme Verlag Stuttgart and Thieme New York; 2015.
4. Östling M, Lubbe N, Jeppsson H, Puthan P. Passenger Car Safety Beyond ADAS: Defining Remaining Accident Configurations as Future Priorities. In: *Proceedings of the International Technical Conference on the Enhanced Safety of Vehicles*. Eindhoven, The Netherlands; 2019.
5. Östling M, Jeppsson H, Lübbe N. Predicting crash configurations in passenger car to passenger car crashes to guide the development of future passenger car safety. In: *Proceedings of the IRCOBI conference*. Florence, Italy; 2019.
6. Renaudin F, Guillemot H, Lavaste F, Skalli W, Lesage F, Pecheux C. A 3D finite element model of pelvis in side impact. *SAE Technical Paper 933130* 1993. doi:10.4271/933130.
7. Plummer JW, Bidez MW, Alonso J. Parametric Finite Element Studies of the Human Pelvis: The Influence of Load Magnitude and Duration on Pelvic Tolerance During Side Impact. In: *Proceedings of the Stapp Car Crash Conference*. Albuquerque, New Mexico, USA; 1996:17–28.
8. Besnault B, Lavaste F, Guillemot H, Robin S, Coz J-Y Le. A Parametric Finite Element Model of the Human Pelvis. *SAE Technical Paper 983147* 1998. doi:10.4271/983147.
9. Konosu A. Development of a biofidelic human pelvic FE-model with several modifications onto a commercial use model for lateral loading conditions. *SAE Technical Paper 2003-01-0163* 2003. doi:10.4271/2003-01-0163.
10. Kikuchi Y, Takahashi Y, Mori F. Development of a Finite Element Model for a Pedestrian Pelvis and Lower Limb. *SAE Technical Paper 2006-01-0683* 2006. doi:10.4271/2006-01-0683.
11. Song E, Trosseille X, Guillemot H. Side Impact: Influence of Impact Conditions and Bone Mechanical Properties on Pelvic Response Using a Fracturable Pelvis Model. *Stapp Car Crash Journal* 2006; **50**:75–95. doi:10.4271/2006-22-0004.
12. Untaroiu CD, Guillemot H, Salzar RS, Crandall JR. The Strain Distribution and Force Transmission Path Through Pubic Rami During Lateral Pelvic Impacts. In: *Proceedings of the IMECE*. Boston, Massachusetts, USA; 2008.
13. Ma Z, Lan F, Chen J, Liu W. Finite Element Study of Human Pelvis Model in Side Impact for Chinese Adult Occupants. *Traffic Injury Prevention* 2015; **16**(4):409–417. doi:10.1080/15389588.2014.950370.
14. Kunitomi S, Yamamoto Y, Kato R, et al. The Development of the Lower Extremity of a Human FE Model and the Influence of Anatomical Detailed Modelling in Vehicle-to-Pedestrian Impacts. In: *Proceedings of the IRCOBI Conference*. Antwerp, Belgium; 2017.
15. Neice R. Master Thesis: Development and Validation of a Pelvis Finite Element Model for Side Panel Intrusion Threats. 2019.
16. Anderson AE, Ellis BJ, Weiss JA. Verification, validation and sensitivity studies in computational biomechanics. *Computer Methods in Biomechanics and Biomedical Engineering* 2007; **10**(3):171–184. doi:10.1080/10255840601160484.
17. Cook D, Julias M, Nauman E. Biological variability in biomechanical engineering research: Significance and meta-analysis of current modeling practices. *Journal of Biomechanics* 2014; **47**:1241–1250. doi:10.1016/J.JBIOMECH.2014.01.040.
18. Naseri H, Iraeus J, Johansson H. The effect of adipose tissue material properties on the lap belt-pelvis interaction: A global sensitivity analysis. *Journal of the Mechanical Behavior of Biomedical Materials* 2020; **107**. doi:10.1016/J.JMBBM.2020.103739.
19. Hu J, Zhang K, Reed MP, Wang J-T, Neal M, Lin C-H. Frontal crash simulations using parametric human models representing a diverse population. *Traffic Injury Prevention* 2019; **20**(sup1):S97–S105. doi:10.1080/15389588.2019.1581926.
20. Iraeus J, Brolin K, Pipkorn B. Generic finite element models of human ribs, developed and validated for stiffness and strain prediction – To be used in rib fracture risk evaluation for the human population in

vehicle crashes. *Journal of the Mechanical Behavior of Biomedical Materials* 2020; **106**. doi:10.1016/J.JMBBM.2020.103742.
21. Perez-Rapela D, Forman JL, Huddleston SH, Crandall JR. Methodology for vehicle safety development and assessment accounting for occupant response variability to human and non-human factors. *Computer Methods in Biomechanics and Biomedical Engineering* 2021; **24**(4):384–399. doi:10.1080/10255842.2020.1830380.
22. Anderson AE, Peters CL, Tuttle BD, Weiss JA. Subject-Specific Finite Element Model of the Pelvis: Development, Validation and Sensitivity Studies. *Journal of Biomechanical Engineering* 2005; **127**(3):364–373. doi:10.1115/1.1894148.
23. O'Rourke D, Martelli S, Bottema M, Taylor M. A Computational Efficient Method to Assess the Sensitivity of Finite-Element Models: An Illustration with the Hemipelvis. *Journal of Biomechanical Engineering* 2016; **138**(12). doi:10.1115/1.4034831.
24. DelPrete H. Similarities in pelvic dimorphisms across populations. *American Journal of Human Biology* 2019; **31**(5):e23282. doi:10.1002/ajhb.23282.
25. Brynskog E, Iraeus J, Reed MP, Davidsson J. Predicting pelvis geometry using a morphometric model with overall anthropometric variables. *Journal of Biomechanics* 2021; **126**. doi:10.1016/J.JBIOMECH.2021.110633.
26. Cesari D, Ramet M. Pelvic Tolerance and Protection Criteria in Side Impact. *SAE Technical Paper 821159* 1982. doi:10.4271/821159.
27. Guillemot H, Got C, Besnault B, et al. Pelvic Behavior in Side Collisions: Static and Dynamic Tests on Isolated Pelvic Bones. In: *Proceedings of the International Technical Conference on the Enhanced Safety of Vehicles*. Windsor Ontario, Canada; 1998.
28. Bouquet R, Ramet M, Bermond F, et al. Pelvis human response to lateral impact. In: *Proceedings of the International Technical Conference on the Enhanced Safety of Vehicles*. Windsor Ontario, Canada; 1998.
29. Salzar RS, Genovese D, Bass CR, et al. Load path distribution within the pelvic structure under lateral loading. *International Journal of Crashworthiness* 2009; **14**(1):99–110. doi:10.1080/13588260802517378.
30. Borgonovo E, Plischke E. Sensitivity analysis: A review of recent advances. *European Journal of Operational Research* 2016; **248**:869–887. doi:10.1016/J.EJOR.2015.06.032.
31. Saltelli A, Ratto M, Andres T, et al. *Global Sensitivity Analysis. The Primer*. Chichester, West Sussex, England: John Wiley & Sons, Ltd; 2008.
32. Saltelli A, Aleksankina K, Becker W, et al. Why so many published sensitivity analyses are false: A systematic review of sensitivity analysis practices. *Environmental Modelling & Software* 2019; **114**:29–39. doi:10.1016/J.ENVSOFT.2019.01.012.
33. Zhang X, Pandey MD. An effective approximation for variance-based global sensitivity analysis. *Reliability Engineering & System Safety* 2014; **121**:164–174. doi:10.1016/J.RESS.2013.07.010.
34. Campolongo F, Saltelli A, Cariboni J. From screening to quantitative sensitivity analysis. A unified approach. *Computer Physics Communications* 2011; **182**:978–988. doi:10.1016/J.CPC.2010.12.039.
35. Al R, Behera CR, Zubov A, Gernaey K V., Sin G. Meta-modeling based efficient global sensitivity analysis for wastewater treatment plants – An application to the BSM2 model. *Computers & Chemical Engineering* 2019; **127**:233–246. doi:10.1016/J.COMPCHEMENG.2019.05.015.
36. Hu J, Fanta A, Neal MON, Reed MP, Wang JTW. Vehicle crash simulations with morphed GHBMC human models of different stature, BMI, and age. In: *Proceedings of the International Digital Human Modeling Conference*. Montreal, Canada; 2016.
37. Harris MD, Anderson AE, Henak CR, Ellis BJ, Peters CL, Weiss JA. Finite element prediction of cartilage contact stresses in normal human hips. *Journal of Orthopaedic Research* 2012; **30**:1133–1139. doi:10.1002/jor.22040.
38. Peretz AM, Hipp JA, Heggeness MH. The Internal Bony Architecture of the Sacrum. *Spine* 1998; **23**(9):971–974. doi:10.1097/00007632-199805010-00001.
39. Richards AM, Coleman NW, Knight TA, Belkoff SM, Mears SC. Bone Density and Cortical Thickness in Normal, Osteopenic, and Osteoporotic Sacra. *Journal of Osteoporosis* 2010. doi:10.4061/2010/504078.
40. Dalstra M, Huiskes R, van Erning L. Development and validation of a three-dimensional finite element model of the pelvic bone. *Journal of Biomechanical Engineering* 1995; **117**(3):272–278. doi:10.1115/1.2794181.
41. Kopperdahl DL, Keaveny TM. Yield strain behavior of trabecular bone. *Journal of Biomechanics* 1998; **31**:601–608. doi:10.1016/S0021-9290(98)00057-8.

42. Kemper AR, McNally C, Duma SM. Dynamic tensile material properties of human pelvic cortical bone. *Biomedical Sciences Instrumentation* 2008; **44**:417–418.
43. Dakin GJ, Arbelaez RA, Molz FJ, Alonso JE, Mann KA, Eberhardt AW. Elastic and Viscoelastic Properties of the Human Pubic Symphysis Joint: Effects of Lateral Impact Loading. *Journal of Biomechanical Engineering* 2001; **123**(3):218–226. doi:10.1115/1.1372321.
44. Ivanov AA, Kiapour A, Ebraheim NA, Goel V. Lumbar Fusion Leads to Increases in Angular Motion and Stress Across Sacroiliac Joint: A Finite Element Study. *Spine* 2009; **34**(5):E162–E169. doi:10.1097/BRS.0b013e3181978ea3.
45. Vleeming A, Schuenke MD, Masi AT, Carreiro JE, Danneels L, Willard FH. The sacroiliac joint: An overview of its anatomy, function and potential clinical implications. *Journal of Anatomy* 2012; **221**:537–567. doi:10.1111/j.1469-7580.2012.01564.x.
46. Steinke H, Hammer N, Slowik V, et al. Novel insights into the sacroiliac joint ligaments. *Spine* 2010; **35**(3):257–63. doi:10.1097/BRS.0b013e3181b7c675.
47. Hammer N, Steinke H, Slowik V, et al. The sacrotuberous and the sacrospinous ligament – A virtual reconstruction. *Annals of Anatomy - Anatomischer Anzeiger* 2009; **191**(4):417–425. doi:10.1016/J.AANAT.2009.03.001.
48. Miller JA, Schultz AB, Andersson GB. Load-Displacement Behavior of Sacroiliac Joints. *Journal of Orthopaedic Research* 1987; **5**:92–101.
49. Hatem MA, da Cunha LAM, Abdo JCM, Martin HD. Parameters for assessment of the inferior acetabulum morphology in 300 adult hips. *Journal of Hip Preservation Surgery* 2016; **4**(1):97–105. doi:10.1093/jhps/hnw040.
50. Milner GR, Boldsen JL. Humeral and Femoral Head Diameters in Recent White American Skeletons. *Journal of Forensic Sciences* 2012; **57**(1):35–40. doi:10.1111/j.1556-4029.2011.01953.x.
51. Šalamon A, Šalamon T, Šef D, Jo-Osvatić A. Morphological characteristics of the acetabulum. *Collegium Antropologicum* 2004; **28**(SUPPL. 2):221–226.
52. Kim DG, Dong XN, Cao T, et al. Evaluation of Filler Materials Used for Uniform Load Distribution at Boundaries During Structural Biomechanical Testing of Whole Vertebrae. *Journal of Biomechanical Engineering* 2006; **128**:161–165. doi:10.1115/1.2133770.
53. Shergold OA, Fleck NA, Radford D. The uniaxial stress versus strain response of pig skin and silicone rubber at low and high strain rates. *International Journal of Impact Engineering* 2006; **32**:1384–1402. doi:10.1016/J.IJIMPENG.2004.11.010.
54. Dalstra M, Huiskes R, Odgaard A, van Erning L. Mechanical and textural properties of pelvic trabecular bone. *Journal of Biomechanics* 1993; **26**(4–5):523–535. doi:10.1016/0021-9290(93)90014-6.
55. Galante J, Rostoker W, Ray RD. Physical Properties of Trabecular Bone. *Calcified Tissue Research* 1970; **5**:236–246.
56. Albert DL, Kang Y, Agnew AM, Kemper AR. A Comparison of Rib Structural and Material Properties from Matched Whole Rib Bending and Tension Coupon Tests. In: *Proceedings of the IRCOBI Conference*. Antwerp , Belgium; 2017.
57. Katzenberger MJ, Albert DL, Agnew AM, Kemper AR. Effects of sex, age, and two loading rates on the tensile material properties of human rib cortical bone. *Journal of the Mechanical Behavior of Biomedical Materials* 2020; **102**. doi:10.1016/J.JMBBM.2019.103410.
58. Albert DL, Katzenberger MJ, Agnew AM, Kemper AR. A comparison of rib cortical bone compressive and tensile material properties: Trends with age, sex, and loading rate. *Journal of the Mechanical Behavior of Biomedical Materials* 2021; **122**. doi:10.1016/J.JMBBM.2021.104668.
59. Nalla RK, Kinney JH, Ritchie RO. Mechanistic fracture criteria for the failure of human cortical bone. *Nature Materials* 2003; **2**:164–168. doi:10.1038/nmat832.
60. Trosseille X, Baudrit P, Leport T, Vallancien G. Rib Cage Strain Pattern as a Function of Chest Loading Configuration. *Stapp Car Crash Journal* 2008; **52**:205–231.
61. Iraeus J, Pipkorn B. Development and Validation of a Generic Finite Element Ribcage to be used for Strain-based Fracture Prediction. In: *Proceedings of the IRCOBI Conference*. Florence, Italy; 2019.
62. Pipkorn B, Iraeus J, Björklund M, Bunketorp O, Jakobsson L. Multi-Scale Validation of a Rib Fracture Prediction Method for Human Body Models. In: *Proceedings of the IRCOBI Conference*. Florence, Italy; 2019.
63. Untaroiu CD, Yue N, Shin J. A finite element model of the lower limb for simulating automotive impacts. *Annals of Biomedical Engineering* 2013; **41**(3):513–526. doi:10.1007/S10439-012-0687-0/FIGURES/13.

64. DeWit JA, Cronin DS. Cervical spine segment finite element model for traumatic injury prediction. *Journal of the Mechanical Behavior of Biomedical Materials* 2012; **10**:138–150. doi:10.1016/J.JMBBM.2012.02.015.
65. Petit P, Trosseille X, Lebarbé M, et al. A Comparison of Sacroiliac and Pubic Rami Fracture Occurrences in Oblique Side Impact Tests on Nine Post Mortem Human Subjects. *Stapp Car Crash Journal* 2015; **59**:23–52.
66. Lebarbé M, Baudrit P, Pascal P, et al. Investigation of Pelvic Injuries on Eighteen Post Mortem Human Subjects Submitted to Oblique Lateral Impacts. *Stapp Car Crash Journal* 2016; **60**:89–134.
67. Natali AN, Meroi EA. A review of the biomechanical properties of bone as a material. *Journal of Biomedical Engineering* 1989; **11**(4):266–276. doi:10.1016/0141-5425(89)90058-7.
68. Khor F, Cronin DS, Watson B, Gierczycka D, Malcolm S. Importance of asymmetry and anisotropy in predicting cortical bone response and fracture using human body model femur in three-point bending and axial rotation. *Journal of the Mechanical Behavior of Biomedical Materials* 2018; **87**:213–229. doi:10.1016/J.JMBBM.2018.07.033.
69. Reilly DT, Burstein AH. The elastic and ultimate properties of compact bone tissue. *Journal of Biomechanics* 1975; **8**(6):393–405. doi:10.1016/0021-9290(75)90075-5.
70. Keaveny TM, Pinilla TP, Crawford RP, Kopperdahl DL, Lou A. Systematic and random errors in compression testing of trabecular bone. *Journal of Orthopaedic Research* 1997; **15**:101–110. doi:10.1002/JOR.1100150115.
71. Helgason B, Perilli E, Schileo E, Taddei F, Brynjólfsson S, Viceconti M. Mathematical relationships between bone density and mechanical properties: A literature review. *Clinical Biomechanics* 2008; **23**:135–146. doi:10.1016/j.clinbiomech.2007.08.024.
72. Li Z, Alonso JE, Kim J-E, Davidson JS, Etheridge BS, Eberhardt AW. Three-Dimensional Finite Element Models of the Human Pubic Symphysis with Viscohyperelastic Soft Tissues. *Annals of Biomedical Engineering* 2006; **34**(9):1452–1462. doi:10.1007/s10439-006-9145-1.

VIII. APPENDIX

A. LS-DYNA specific modelling

TABLE A I

LS-DYNA SPECIFIC DETAILS ON ELEMENT FORMULATION AND MATERIAL MODEL FOR INCLUDED STRUCTURES.

Structure	Element formulation	Material model
Trabecular bone	Constant stress solid element (ELFORM = 1)	*MAT_PIECEWISE_LINEAR_PLASTICITY (MAT_024)
Cortical bone	Fully integrated shell element (ELFORM = 16)	*MAT_PIECEWISE_LINEAR_PLASTICITY (MAT_024)
Pubic symphysis disc	Fully integrated S/R solid for elements with poor aspect ratio (ELFORM = -2)	*MAT_SIMPLIFIED_RUBBER/FOAM (MAT_181)
Pubic symphysis ligaments	Fully integrated shell element (ELFORM = 16)	*MAT_SIMPLIFIED_RUBBER/FOAM (MAT_181)
SI articular cartilage	Fully integrated S/R solid for elements with poor aspect ratio (ELFORM = -2)	*MAT_SIMPLIFIED_RUBBER/FOAM (MAT_181)
Interosseous ligaments	Fully integrated S/R solid for elements with poor aspect ratio (ELFORM = -2)	*MAT_SIMPLIFIED_RUBBER/FOAM (MAT_181)
Anterior SI, posterior SI, sacrotuberous, and sacrospinous ligaments	Discrete beam/cable (ELFORM = 6)	*MAT_CABLE_DESCRETE_BEAM (MAT_071)
Acetabulum articular cartilage	Fully integrated S/R solid for elements with poor aspect ratio (ELFORM = -2)	*MAT_SIMPLIFIED_RUBBER/FOAM (MAT_181)
Silicone padding (dynamic case)	Constant stress solid element (ELFORM = 1)	*OGDEN_RUBBER (MAT_077_O)

TABLE A II

LS-DYNA SPECIFIC DETAILS ON CONTACT AND CONSTRAINT FORMULATIONS FOR INCLUDED STRUCTURES.

Interacting structures	Contact formulation	Specific settings
Interosseous ligament solids to innominate cortical bone shells	*TIED_SHELL_EDGE_TO_SOLID_BEAM_OFFSET	Interosseous node set to cortical shell PID SOFT = 0
SI articular cartilage NULL shells to innominate cortical bone shells	*AUTOMATIC_SURFACE_TO_SURFACE	Cartilage NULL shell PID to cortical shell PID FS = FD = 0.3 SFS = SFM = 10 SOFT = 2, SBOPT = 3, DEPTH = 5
Rigid plate to iliac wing	*AUTOMATIC_SURFACE_TO_SURFACE	Rigid shell PID to cortical shell PID FS = FD = 0.1 SOFT = 2, SBOPT = 3, DEPTH = 5
Rigid sphere to acetabulum	*AUTOMATIC_SURFACE_TO_SURFACE	Rigid shell PID to cortical shell and acetabulum cartilage set FS = FD = 0.1 SOFT = 2, SBOPT = 3, DEPTH = 5
Rigid sphere to silicone padding	*AUTOMATIC_SURFACE_TO_SURFACE	Rigid shell PID to silicone solid PID FS = FD = 0.1

Interacting structures	Constraint formulation
Innominate bone shells to casting solids	*CONSTRAINED_SHELL_IN_SOLID_PENALTY

B. Modelling and calibration of the pubic symphysis joint

Experiment

Reference [43] performed component tests on twenty pubic symphysis specimens (13 males, 7 females) harvested from unembalmed PMHSs aged 41 to 93 years (average 65.7 years). The joint was laterally sectioned on all four pubic rami approximately 4 cm from the pubic disc before it was potted such that the disc was oriented perpendicular to and centred within the top surface of the aluminium pots.

For axial tension and compression testing, the bottom centre of one pot was securely attached while the other was loaded. Preconditioning was performed by loading the joint for a series of ten linear ramp displacements (1 mm/s) to an amplitude of ±0.8 mm before tension and compression stiffnesses were measured. A stiffness toe region was defined as 0 to 10% of the loading curves while the linear region was defined as 80 to 90%. Mean and one standard deviation of toe and linear stiffness for each direction were presented in a table [43]. Force-displacement curves were not shown by [43] but a later article by [72] presented average female/male compression-tension curves based on the same experiments.

Simulation Setup and Calibration

The pubic bones were cut approximately 4 cm from the pubic disc and placed in boxes to replicate the potting, see Fig. B 1. The cast was simulated using *CONSTRAINED_SHELL_IN_SOLID_PENALTY and hexahedral elements with a linear elastic polymethyl-methacrylate material (E = 2.85 GPa). The bottom pot was constrained while the top pot was moved at 1 mm/s to an amplitude of ±1.0 mm. The model was morphed to the female/male baseline geometries to compare with the female/male experimental results. The compression-tension curves of the disc and ligaments were manually calibrated to fit the experimental response, see Fig. B 2 to Fig. B 4.

Results

The resulting compression-tension curves for the female/male models can be seen in Fig. B 5 while toe and linear average responses are presented in Fig. B 6. In tension, the experiment average female linear response was 543 N (SD=77 N), while the average male linear response was 816 N (SD=320 N). From simulation, the female response was 627 N and the male response 957 N. In compression, the experiment average female linear response was 1158 N (SD=337 N), while the average male linear response was 1581 N (SD=676 N). From simulation the female response was 1423 N and the male response 1861 N.

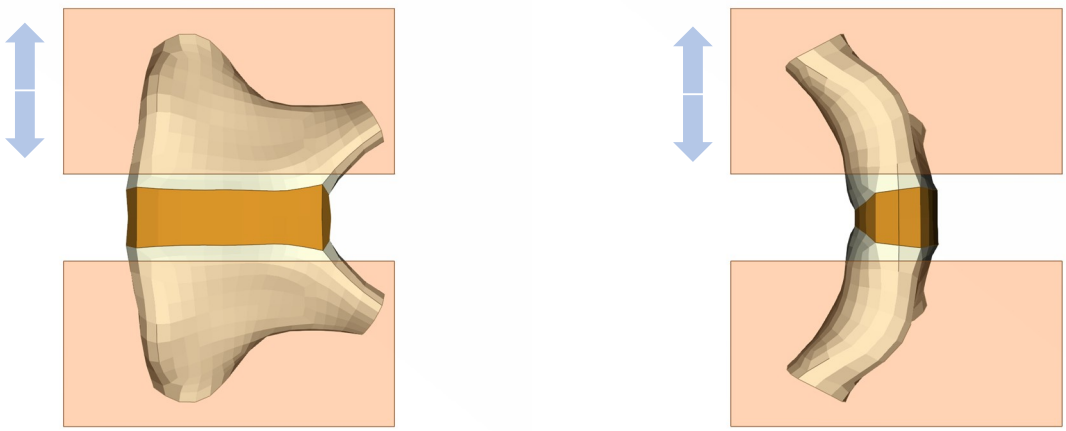

Fig. B 1. Simulation setup, anterior view (left), superior view (right).

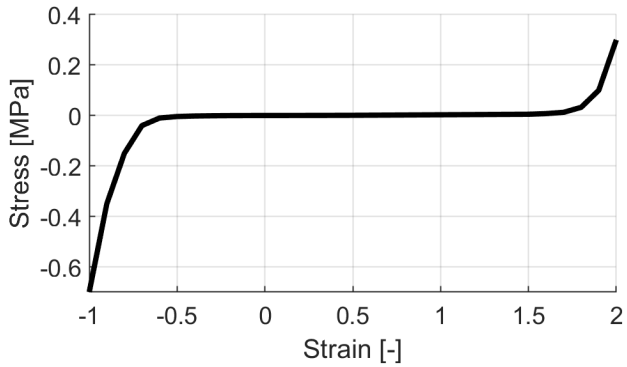

Fig. B 2. Full compression-tension curve of pubic symphysis disc.

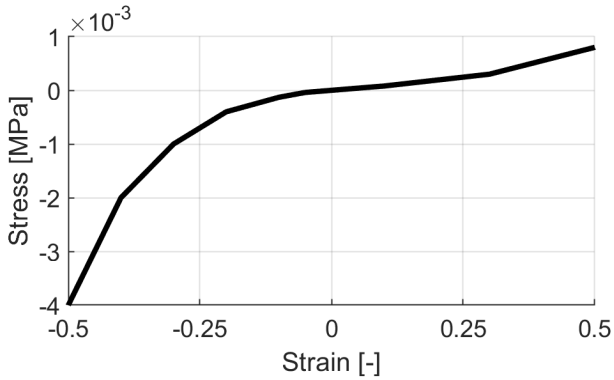

Fig. B 3. Compression-tension curve of pubic symphysis disc in strain range [-0.5, 0.5].

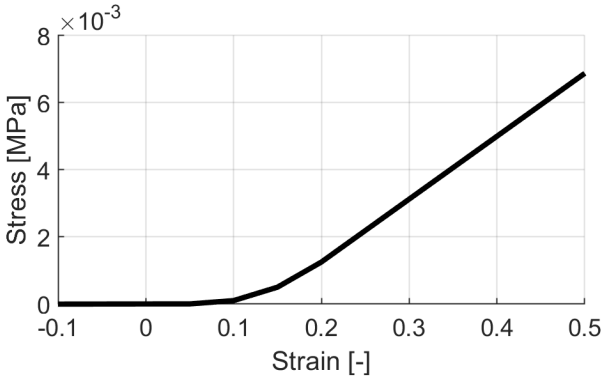

Fig. B 4. Compression-tension curve of pubic symphysis ligament, curve continues linearly past 0.5.

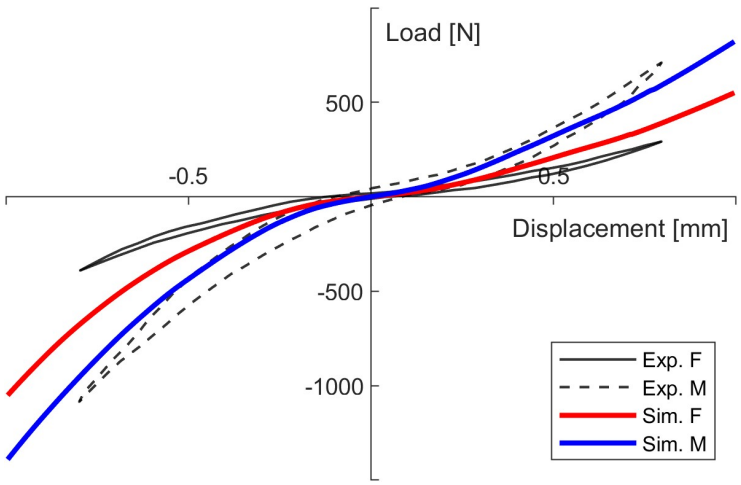

Fig. B 5. Female/male compression-tension curve compared with average from experiments.

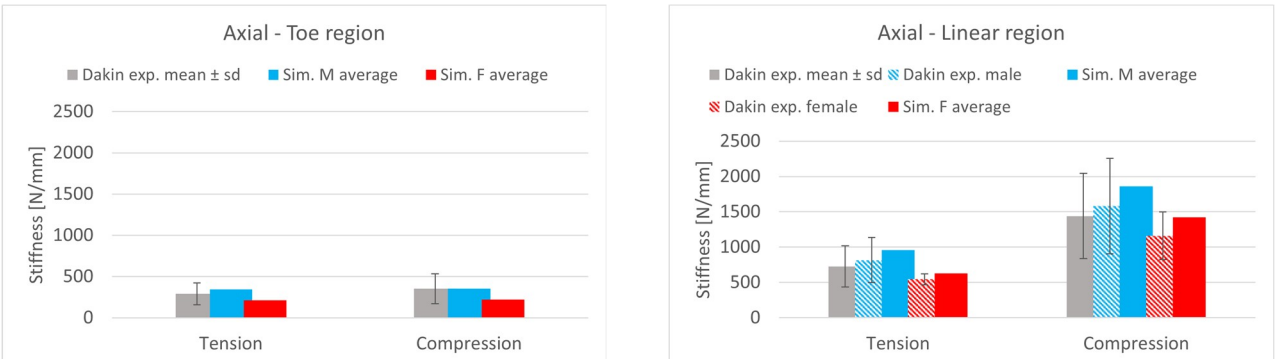

Fig. B 6. Average (±SD) results from experiments compared with simulation response, toe region (left), linear region (right).

C. Modelling and validation of the sacroiliac joint

Experiment

Reference [48] performed component tests on eight fresh bilateral SI joint specimens (7 males, 1 female) aged between 59 and 74 years (mean 66 years). Each ilium was sectioned approximately 10 cm lateral to the SI joint. Specimens were freed from all muscular tissue and the sacral spinous processes were removed. Each ilium was then cast into a block of cement while steel plates were mounted on the anterior and posterior surface of the sacrum using steel wires and a central bolt. To improve fixation, cement was placed between the plates and the sacral surface. A loading arm was attached normal to each plate through which forces and moment could be applied in three orthogonal directions through the centre of the sacrum. The centre of the sacrum was defined as lying in the midsagittal plane, midway between the inferior S1 and superior S2 vertebrae endplates and the anterior and posterior margins of the auricular SI joint surfaces viewed laterally. The mean value of the centre of the sacrum was 29.0 mm inferior and 11.5 mm posterior of the centre of the superior S1 endplate.

With both ilia fixed, a force of 294 N or a torque of 42 Nm were applied to the sacrum. These loads were applied in the following order: anterior, posterior, flexion, extension, superior, inferior, axial torsion, lateral bending, and medial. One ilium was then released from the test stand, and the full sequence repeated. Results are presented as mean and one standard deviation displacement/rotation for the force/torque loading respectively.

Simulation Setup

The innominate bones of the pelvis were cut to replicate the experiment and all soft tissues, except for the SI-joints, were removed. The left and right innominate bone and the S1 and S2 vertebrae bodies were then placed in boxes to replicate the cement casting, see Fig. C 1. To constrain the bones in each box *CONSTRAINED_SHELL_IN_SOLID_PENALTY was used. The centre of sacrum was defined based on the average values in the article and a node called origo was placed at this point for load application. A local coordinate system was defined at origo with its X-axis along the surface of the S1 endplate in the anterior-posterior direction and Z-axis as the normal of the endplate surface. The force (294 N) and torque (42 Nm) was applied to the origo node in the directions of the local coordinate system. Since the displacements with both ilia fixed were so small in the experiments, the one ilium fixed results were prioritised for validation. The measured response was the displacement and rotations of origo in the local coordinate system. To check sensitivity, both the female and male baseline were simulated.

Results

The displacement and rotation of the origo node, in the direction of the load, can be seen in Fig. C 2. For all force loadings, except anterior force, lateral torque, and female flexion/extension, the response was within ±1 SD for both the female and male baseline. In the anterior force case, the model response was too stiff compared with the experiments, while in the lateral torque and female flexion/extension cases, the model was slightly too weak. Despite several attempts to fix these contradicting demands, a version with all response metrics within ±1 SD was not achieved. However, this is not expected to have a significant effect on the general conclusions of this paper.

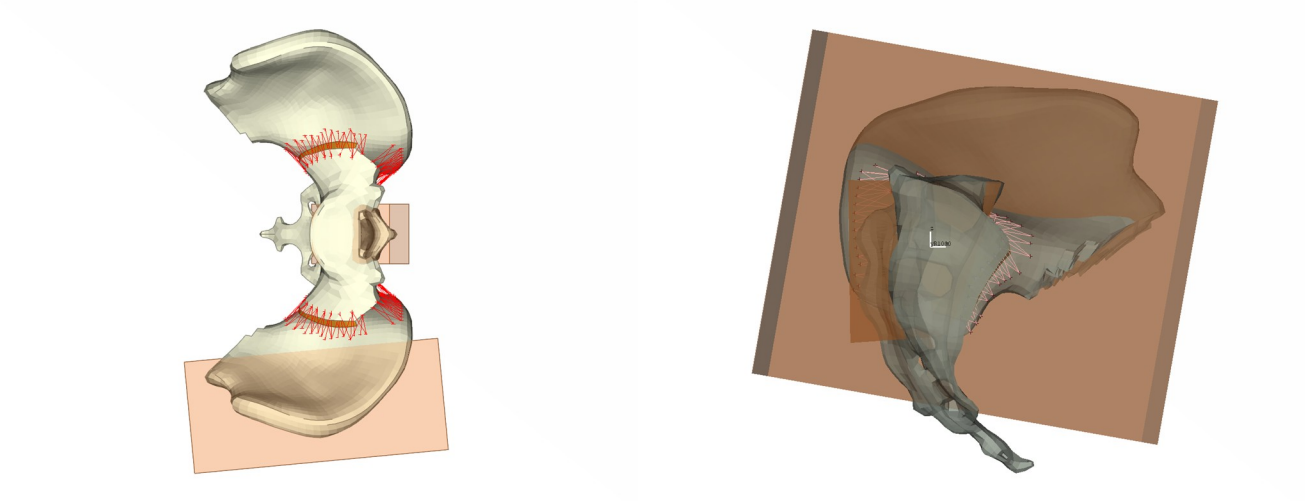

Fig. C 1. Simulation setup for one ilium fixed, superior view (left), lateral view (right) with origo coordinate system highlighted.

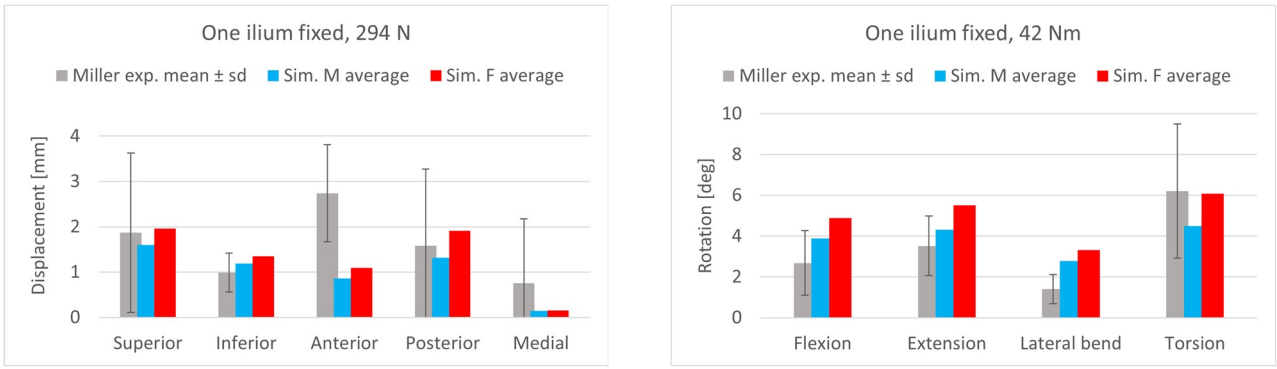

Fig. C 2. Displacement (left) and rotation (right) response from applied force and torque load.

D. Mesh quality criteria

TABLE D I

MESH QUALITY CRITERIA USED WHEN DEVELOPING THE AVERAGE FE-MODEL (SOFTWARE WITHIN BRACKETS DEFINES CRITERIA). SUPER SCRIPTS REFERS TO PUBLICATIONS OR OTHER SOURCES USED AS BASIS FOR CRITERIA LEVELS. THE 100% LIMIT IS MAINLY FOR OVERALL MODEL STABILITY AND SHOULD THUS BE FULFILLED FOR THE WHOLE MODEL. THE 95% TARGET IS NOT A STRICT LIMIT, RATHER AN AMBITION. AREAS OF HIGH IMPORTANCE, WHERE TISSUE-BASED INJURY CRITERIA SHOULD BE USED, ARE PRIORITISED TO FULFIL THIS TARGET.

Solid Elements	Aspect Ratio [-] (Patran)	Skewness [deg] (Patran)	Warpage [deg] (Patran)	Hexa Angle [deg] (Abaqus)	Tetra Angle [deg] (Abaqus)	Jacobian [-] (ANSA)
95% Target	<3[a]-[c]	<45[b]	<10[c]	30<ϕ<140[c]	30<ϕ<120[b]	>0.7[a], [c]
100% Limit	<10 [a],[c]	<60[b]	<20[b]	20<ϕ<160[a]	20[c]<ϕ<150[a]	>0.3[c]

Shell elements	Aspect Ratio [-] (Patran)	Skewness [deg] (Patran)	Warpage [deg] (Patran)	Quad Angle [deg] (IDEAS)	Tria Angle [deg] (IDEAS)	Jacobian [-] (ANSA)
95% Target	<3[a]-[c]	<30[c]	<7[c]	45<ϕ<135[b], [c]		>0.7[a], [c]
100% Limit	<10[b]	<60[b]	<20[b]	20<ϕ<160[c]	30<ϕ<120[b], [c]	>0.3[c]

[a] Burkhart, T. A., Andrews, D. M., & Dunning, C. E. (2013). Finite element modeling mesh quality, energy balance and validation methods: a review with recommendations associated with the modeling of bone tissue. *Journal of biomechanics, 46*(9), 1477-1488

[b] Yang, K.-H. (2017). *Basic finite element method as applied to injury biomechanics*: Academic Press.

[c] Industry requirements

TABLE D II

MESH QUALITY OF THE AVERAGE PELVIS FE-MODEL AND THE FEMALE / MALE BASELINES. THE TABLE SHOWS THE PERCENTAGE OF ELEMENTS FULFILLING THE 95% TARGETS, ALL ELEMENTS IN THE AVERAGE FE-MODEL FULFILLED THE 100% LIMITS.

	Nr. of Elements	Aspect Ratio	Skewness	Warpage	Hexa / Quad Angle	Jacobian
Solid Elements						
Average pelvis	23,926	88.2%	90.3%	92.2%	88.2%	92.8%
Female baseline	23,926	88.1%	90.0%	92.1%	88.0%	92.7%
Male baseline	23,926	88.5%	89.8%	92.3%	87.4%	92.8%
Shell elements						
Average pelvis	10,812	99.6%	95.1%	94.4%	97.2%	97.2%
Female baseline	10,812	99.5%	93.1%	94.6%	97.1%	97.1%
Male baseline	10,812	99.1%	91.3%	94.2%	96.8%	97.1%

E. Mesh quality criteria

To check how the choice of strain response metric affected the conclusions, the analysis was also carried out with nodal averaged 1st principal strain and nodal averaged effective strain. Fig. E 1 shows the resulting primary sensitivity indices while Fig. E 2 shows the summation as shape, material, cortical thickness, and interaction. Some minor differences can be seen depending on the chosen metric, but the final conclusions drawn would not be affected by this choice.

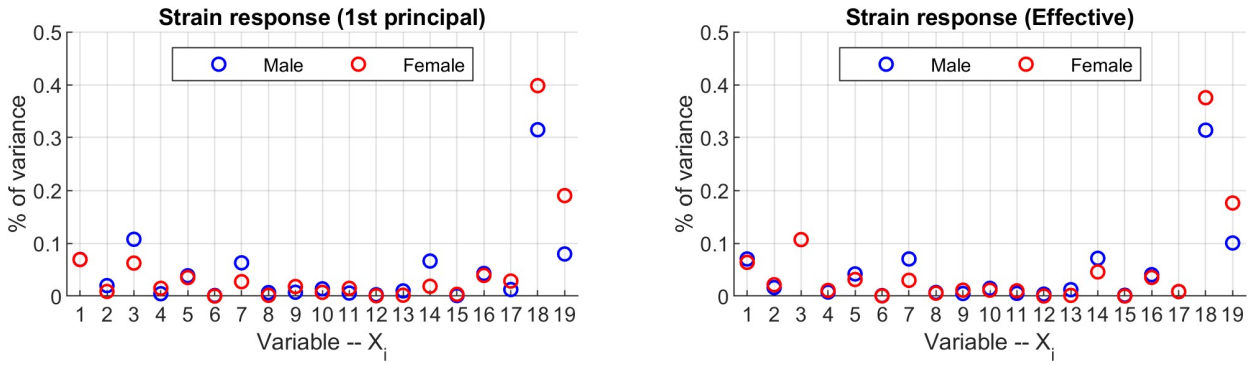

Fig. E 1. Primary sensitivity indices for the female/male baseline model using nodal averaged 1st principal strain (left) and nodal averaged effective strain (right) in the superior pubic rami as evaluation metric. Variable 1-15 = PC1-15, Variable 16 = scale, Variable 17 = trabecular bone apparent density (used to compute Young's modulus), Variable 18 = cortical bone Young's modulus, and Variable 19 = cortical thickness.

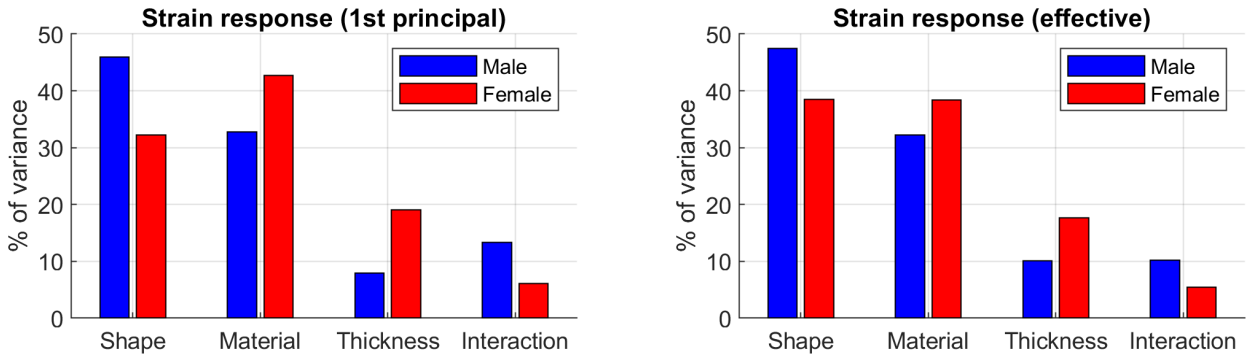

Fig. E 2. Summation of primary sensitivity indices relating to shape (Variable 1-16), material (Variable 17-18), and cortical thickness (Variable 19), together with remaining interaction effects for a female/male baseline model using nodal averaged 1st principal strain (left) and nodal averaged effective strain (right) in the superior pubic rami as evaluation metric.